THE JOURNAL OF PHYSICAL CHEMISTRY A

Article

pubs.acs.org/JPCA

Mechanisms of Propylene Glycol and Triacetin Pyrolysis

Teodoro Laino,*[,†] Christian Tuma,[†] Philippe Moor,[‡] Elyette Martin,[‡] Steffen Stolz,[‡,§] and Alessandro Curioni[†]

[†]IBM Research−Zurich, Säumerstrasse 4, 8803 Rüschlikon, Switzerland

[‡]Philip Morris International R&D, Quai Jeanrenaud 5, 2000 Neuchâtel, Switzerland

[§]University of Twente, Faculty EEMCS, P.O. Box 217, 7500 AE Enschede, The Netherlands

Supporting Information

ABSTRACT: Propylene glycol and triacetin are chemical compounds, commonly used as food additives. Though the usage of the pure chemicals is not considered harmful when used as dietary supplements, little is known about the nature of their thermal degradation products and the impact they may have on human health. For these reasons, in this manuscript we investigate the thermal decomposition mechanisms of both neutral propylene glycol and triacetin in the gas phase by a novel simulation framework. This is based on a free energy sampling methodology followed by an accurate energy refinement. Structures, Gibbs free energy barriers, and rate constants at 800 K were computed for the different steps involved in the two pyrolytic processes. The thermal decomposition mechanisms found theoretically for propylene glycol and triacetin were validated by a qualitative experimental investigation using gas-phase chromatography−mass spectroscopy, with excellent agreement. The results provide a validation of the novel simulation framework and shed light on the potential hazard to the health that propylene glycol and triacetin may have when exposed to high temperatures.

INTRODUCTION

Propylene glycol (propane-1,2-diol, PG) and triacetin (propane-1,2,3-triyl triacetate, TA) are hygroscopic organic compounds. Both PG and TA, commercially known as E1520 and E1518, are widely used as solvents in pharmaceutical formulations, as humectants and plasticizers in food additives, and as moisturizers in medicine, cosmetics, food, and the tobacco industry. TA has also been extensively used as fuel additive, improving the fuel's cold flow properties and reducing the knocking of gasoline-based engines. PG and TA can be considered the simplest possible carbohydrate (PG) and fat (TA) after glyceryl triformate. For these reasons their chemistry is of paramount importance, being prototypical for larger and more complex structures. Owing to the lack of evidence of being either carcinogenic or genotoxic, both PG and TA are not considered harmful for human health.[1] Because of that, they have been suggested as a possible source of food energy in artificial food regeneration systems on long space missions.

However, for their pyrolytic products, the scenario is entirely different. In fact, as is well-known from the biomass community, PG, under specific catalytic conditions, can efficiently dehydrate into propanal,[2] a potentially harmful substance. Furthermore, very little is known about the pyrolytic processes governing the decomposition of TA and, most importantly, about the chemical species formed under pyrolytic conditions.

The pyrolysis of PG has been the subject of several recent experimental studies.[2−5] Mori et al.[2] investigated the vapor-phase catalytic dehydration of PG over several catalysts, all characterized by acidic properties. They found that the deoxygenation of PG is strongly influenced by high concentrations of acid, giving faster rates and proceeding to higher conversions. Propanal was observed as an intermediate, being formed through acid-catalyzed dehydration of PG. Additional studies[3,5] have characterized the reactivity of PG in the presence of oxidizing/reducing agents. In particular, Diaz et al.[3] investigated the oxidation of PG in the presence of O_2 at 400−500 K. They found that PG forms propanal, formaldehyde, and carbon dioxide via oxidative C−C bond cleavage, as well as acetone via dehydration routes. The products formed and their kinetic dependence on reactant concentrations are consistent with radical-mediated pathways initiated by O_2^{2-} insertion into C−H bonds in a β-position relative to oxygen atoms in diol reactants. Propagation involves β-scission reactions that form hydroxyl and hydroxyalkyl radicals. By comparison with triols and alkanols, Diaz et al.[3] revealed the unique reactivity of diols in homogeneous oxidation conditions, providing useful insights into the molecular basis for reactivity in biomass-derived oxygenates. Huang et al.[5] explored the

Received: January 31, 2012
Revised: April 18, 2012
Published: April 18, 2012

deoxygenation of PG catalyzed by a ruthenium complex at 383 K under hydrogen (5.2 MPa), leading to *n*-propanol as the major product, indicating high selectivity for deoxygenation of the internal hydroxyl group over the terminal hydroxyl group of the diol.

Recently, Zy et al.[4] carried out dehydration experiments of PG in near-critical water conditions to study the reactivity of diol under high temperature and pressure. They identified 2-methyl-2-pentenal (MP) as the final product, with a yield of 1.8 wt %, reporting two possible mechanisms as the characteristic ones leading to the decomposition of PG: the pinacol rearrangement and the elimination reaction. They also explored the catalytic properties of zinc chloride ($ZnCl_2$) and sodium carbonate (Na_2CO_3), finding that whereas $ZnCl_2$ promotes the dehydration of PG, Na_2CO_3 suppresses it.

From a computational perspective, and to the best of our knowledge, there is only one study that explores the conversion of PG to propanal and propanone under various acid-catalyzed reaction conditions.[6] Using density functional theory (DFT, B3LYP), Rungnim et al.[6] studied the dehydration of protonated PG, investigating the pinacol rearrangement conversion to propanal and propanone in the presence of several water molecules. Regarding triacetin, we are not aware of any computational or experimental study related to its pyrolytic chemistry.

Despite several types of investigations published in the literature, it is remarkable that there has been no attempt to characterize the decomposition of pure PG and pure TA in the gas phase. This is of paramount importance, because it offers a deep understanding on how easily PG and TA can decompose at high temperature and on the types of chemical products potentially forming during the degradation processes. In this article we present a computational study of the dehydration of PG inspired by our recent work,[7] which revisited the mechanism of glycerol pyrolysis. Similarly to what has been proposed for glycerol,[7,8] we hypothesize that PG can dehydrate into propylene oxide (an oxirane intermediate), which is then converted further into either propanal or acetone, whereas for TA, the pyrolysis mechanism is hypothesized to be driven either by acetic anhydride or acetic acid elimination, with the latter being the energetically favored step according to our findings.

The simulation framework consisted of the exploration of the potential energy surfaces related to the pyrolytic decomposition of both PG and TA in vacuum by means of the metadynamics[9,10] technique. The reactive trajectories were optimized with the nudged elastic band algorithm,[11] and on selected points of the minimum energy path, energies were refined at the DFT level, employing the hybrid PBE0[12] functional. This simulation allows us to retrieve highly accurate thermodynamic and kinetic properties of the different reaction steps.

The outcome of our simulation framework will be presented in detail, and for each degradation step, rate constants $k(T)$, obtained from canonical transition-state theory,[13−17] will be provided. This is the first time that the challenging decomposition pattern of triacetin is explored by means of ab initio methodologies, providing a complex picture with several decomposition channels.

As a validation to our calculations, we have performed, after completion of the computational investigation, a pyrolysis−gas chromatography−mass spectrometry study for pure propylene glycol and pure triacetin to characterize the products of the high-temperature decomposition pathways. Components separated by gas chromatography (GC) are identified by comparing their characteristic mass spectrometry (MS) fingerprints with a molecular database. These experimental data, discussed in the context of the calculations, provide good support for the modeling from first principles and complement the overall decomposition schemes.

■ COMPUTATIONAL DETAILS

The characterization of the high-temperature molecular degradation processes in the gas phase requires a simulation framework robust enough to explore different reaction channels and able to provide accurate energetics for computing thermodynamic and kinetic quantities. Although the exploration requires a compromise between the computational cost of the Hamiltonian model and the accuracy of the underlying potential energy surface, the refinement of the energies is tightly connected to the usage of a reliable and robust Hamiltonian model. For this reason, we devised a novel simulation framework based on the exploration of the free energy surfaces by means of metadynamics simulations,[9,10] followed by optimization of the corresponding minimum energy path (MEP), with further refinement of selected MEP points at the DFT level with the usage of the hybrid PBE0[12] functional.

In fact, in contrast to standard quantum chemical approaches, where results strongly depend on the chemical intuition used in building the model, metadynamics simulations[9,10] sample the potential energy space with respect to a set of internal (collective) variables in a more unbiased way. Therefore, they can be considered a useful exploratory tool that offers the advantage of providing reactive trajectories which follow the minimum energy path projected in the space of collective variables. This is of paramount importance when the study focuses on systems having a large number of degrees of freedom like in the case of TA.

Free-energy surfaces were sampled according to the following strategy. Using a density functional theory (DFT, PBE,[18] 80 Ry plane-wave basis set cutoff and norm-conserving atomic pseudopotentials[19]) Hamiltonian and metadynamics[9,10] simulations with a set of appropriately chosen collective variables, the free energy spaces of PG and TA were sampled to search for low-barrier reactive events. The collective variables were all related to the coordination of oxygen with hydrogen and carbon atoms, describing a water molecule connected either to the propylene glycol moiety or to dehydrated PG. The functional form used to describe the coordination variable, as implemented in the CPMD[20] code, is

$$s(O_1,C_1,C_2,C_3) = \frac{1}{2}\left\{ \frac{1-\left(\frac{R_{O_1C_1}}{R_0}\right)^6}{1-\left(\frac{R_{O_1C_1}}{R_0}\right)^{12}} + \frac{1-\left(\frac{R_{O_1C_2}}{R_0}\right)^6}{1-\left(\frac{R_{O_1C_2}}{R_0}\right)^{12}} + \frac{1-\left(\frac{R_{O_1C_3}}{R_0}\right)^6}{1-\left(\frac{R_{O_1C_3}}{R_0}\right)^{12}} \right\} \quad (1)$$

Here, $R_{O_iC_j}$ are the distances between a selected oxygen (i) and the carbon atoms (j) of the PG moiety. R_0 is the equilibrium distance of an oxygen−carbon bond in PG (1.55 Å). For TA, we used several distances as collective variables to describe the

dx.doi.org/10.1021/jp300997d | J. Phys. Chem. A 2012, 116, 4602−4609

removal of acetate groups. To sample reactive events, we have employed metadynamics, for both PG and TA, in turn with standard constrained molecular dynamics.

The reactive trajectories were then optimized using a climbing image nudged elastic band (NEB)[11] approach with 20 images sampling the reactive path. These calculations were performed using the CP2K code[21] and a semiempirical PM6[22] Hamiltonian.

Starting from selected points of the PM6 optimized reactive paths, stationary points corresponding to reactants, transition structures and products were located using DFT with the PBE0[12] parameter-free hybrid exchange−correlation functional. In these calculations, a plane-wave basis set with a 100 Ry kinetic energy cutoff was employed, combined with norm-conserving atomic pseudopotentials.[19] Periodic images of the molecules were decoupled using a Poisson solver[23] with cubic computational boxes of 15 Å edge length for PG and 21 Å for TA. Convergence was achieved in structure relaxations when all Cartesian force components became smaller than 2.0×10^{-5} atomic units. Force constant matrices (Hessians) were computed by numerical differentiation of analytical forces. Translations and rotations were projected out from the Hessian. Stationary points were characterized on the basis of the corresponding vibrational frequencies. Reactants and products of each reactive step had no imaginary frequencies whereas transition structures had exactly one. In addition, transition structures were inspected by intrinsic reaction coordinate (IRC) calculations[24] in both directions to retrieve either the reactants or the products. These calculations were performed using the CPMD code.[20]

The evaluation of the reaction rate constants $k(T)$ was carried out within canonical transition-state theory formalism

$$k(T) = \frac{k_B T}{h} \exp\left(-\frac{\Delta G^{\ddagger}(T)}{RT}\right) \quad (2)$$

where k_B is the Boltzmann constant, h is Planck's constant, $\Delta G^{\ddagger}(T)$ is the activation Gibbs free energy barrier of the reaction at a given temperature T, and R is the gas constant. Finite temperature entropy and enthalpy contributions were obtained from standard statistical mechanics approaches.

EXPERIMENTAL DETAILS

Materials. Propylene glycol (>99.5%) and triacetine (>99.0%) were purchased from Sigma-Aldrich and were used for pyrolysis experiments without further purification.

PG and TA Pyrolysis. Pyrolysis analyses were carried out with a CDS 5200 pyroprobe (CDS Analytical) coupled to a 6890 Series GC (Agilent) with CO_2 cryogenic option and a 5973 Series MSD (Agilent). The pyroprobe device was configured in direct pyrolysis mode. Pyrolyses were performed at 800 K for 30 s with an interface temperature of 543 K to prevent condensation in the pyrolysis chamber. Conditions: pyrolysis atmosphere, He; pyrolysis chamber gas flow, 15 mL/min. The pyrolysis products were injected into the GC via a fused silica transfer line heated at 553 K. The transfer line was connected to the split/splitless GC injector heated at 553 K. The injector was operated in split mode with a split ratio of 1:15. Conditions: carrier gas, He; inlet pressure at 278 K, 82 kPa; constant-flow mode. Separation was performed on a CPSil 8CB low-bleed MS capillary column (Chrompack): 50 m, 0.25 mm i.d., 0.40 μm film thickness. Oven temperature program: 278 K (hold 2 min), heating rate 5 K/min up to 553 K (hold 20 min). MSD temperatures: source 503 K, quad 423 K. EI mode: 70 eV. Mass range 15−600 amu.

Pyrolysis tubes were prepared by inserting a quartz wool plug of approximately 2 mm length into the CDS pyro-probe quartz tubes. The tubes were heated in a blue flame for cleaning, and blank runs were performed to ensure absence of contamination in the analytical system. A 0.5 μl quantity of sample was applied to the quartz wool plug with a GC syringe. Two replicates per sample were performed. Pyrolysis compounds were identified by comparing their mass spectra with those of reference compounds from the Wiley and NIST libraries.[25]

The MS response factor of the different chemical species was not determined. Consequently, the chromatograms cannot be interpreted quantitatively.

RESULTS AND DISCUSSION

Here we describe the individual reaction steps that represent the decomposition pathways for the pyrolysis of PG and TA together with the activation Gibbs free energy barriers computed for a temperature T of 800 K.

Whereas the decomposition pathway can be considered exhaustive for the case of PG, the large number of degrees of freedom for TA imposes some constraints in the exploration of the phase space for this molecular unit. By employing the simulation framework described above, we sampled the most favorable decomposition pathways accessible at a temperature of 800 K, providing, to the best of our analysis, exhaustive degradation processes both for PG and TA. Nonetheless, specifically for the complex degradation process of TA, we cannot exclude a priori the presence of additional reactive paths not sampled by our simulation framework.

In the following, we describe the entire set of reactive events observed in our simulations.

Propylene Glycol. Propylene glycol (**1**) has been found to decompose according to three possible reaction pathways shown in Scheme 1. With a barrier of 91.0 kcal/mol, the first route is a dehydration reaction leading to allyl alcohol (**5**). The other two possible degradation schemes involve the formation of propylene oxide (**2**) as an intermediate, which can be formed much more easily than **5** by overcoming a reaction barrier of only 66.5 kcal/mol. Via hydrogen shift, propylene oxide (**2**) can decompose further, forming acetone (**3**) or propanal (**4**) with barriers of 67.0 and 58.6 kcal/mol, respectively. It can be concluded that propanal is the main product of the thermal decomposition of PG. Table 1 summarizes the thermodynamic and kinetic data computed for T = 800 K. Compared with our study on the thermal decomposition of glycerol, where exactly the same methodology was employed,[7] we find that PG exhibits a thermal stability very similar to that of glycerol. With values of

Scheme 1. Decomposition of Propylene Glycol

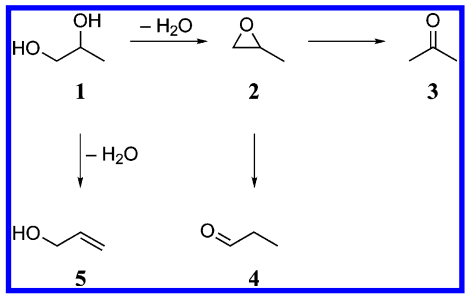

dx.doi.org/10.1021/jp300997d | J. Phys. Chem. A 2012, 116, 4602−4609

Table 1. DFT/PBE0 Total Energy ($\Delta E^{\ddagger}$), Zero-Point Vibrational Energy Corrected ($\Delta E_0^{\ddagger}$), Enthalpy ($\Delta H^{\ddagger}(T)$), and Gibbs Free Energy ($\Delta G^{\ddagger}(T)$) Barrier Heights (kcal/mol) as Well as Rate Constants $k(T)$ (s^{-1}) Computed for the Reaction Steps of the PG Decomposition Depicted in Scheme 1 (T = 800 K)

reaction step	$\Delta E^{\ddagger}$	$\Delta E_0^{\ddagger}$	$\Delta H^{\ddagger}(T)$	$\Delta G^{\ddagger}(T)$	$k(T)$
1 → 2	71.0	66.8	66.5	66.5	1×10^{-5}
2 → 3	72.1	67.9	68.3	67.0	8×10^{-6}
2 → 4	63.4	59.5	59.5	58.6	2×10^{-3}
1 → 5	94.1	90.2	90.4	91.0	2×10^{-12}

66.8 kcal/mol (ref 7) and 66.5 kcal/mol (Table 1), the corresponding rate limiting steps (the epoxide formation in both cases) show virtually the same barrier heights.

In Scheme 2, we report the gas chromatogram of the pyrolytic products of propylene glycol. Although the data cannot be interpreted quantitatively, we can still compare the results with the theoretical predictions from a qualitative point of view. The first relevant item to compare is the amount of nonpyrolyzed propylene glycol. The GC spectrum shows that after exposure to 800 K almost 99.9% of pure PG is recovered. This is in good agreement with the kinetic constant obtained from our computations: the PG pyrolytic degradation is slow at 800K. Furthermore, each of the products predicted is identified.

In the spectrum, we also observe the presence of 1-hydroxy-2-propanone, which was not predicted by our simulations. The presence of air and water may have promoted the oxidation of acetone into 1-hydroxypropanone via a secondary bimolecular degradation pathway that is not covered in our simulations foFcused on unimolecular degradation steps in general. Overall, the experimental analysis, performed to validate the computational modeling, offers an excellent validation of our setup, confirming all theoretically predicted compounds.

Triacetin. Because of the molecular size of triacetin, and in particular the presence of three ester groups, the TA decomposition pathway is complex in nature. Compared with propylene glycol or glycerol, the main decomposition routes are driven by the elimination of acetic acid, acetic anhydride, or ethenone. Analyzing our simulation data we were able to rationalize the possible decomposition steps of TA into three major schemes or branches. The first includes decomposition routes based on the elimination of acetic acid from TA (Scheme 3), the second covers decomposition pathways starting from the elimination of acetic anhydride (Scheme 4), and the third is related to the elimination of ethenone from triacetin ester groups. We did not study subsequent steps for the thermal decomposition of acetic acid or acetic anhydride because data for these systems are available from the literature.[26−30]

Branch I. Triacetin Decomposition by Elimination of Acetic Acid (Scheme 3). With a barrier of 46.1 kcal/mol, acetic acid can be eliminated from triacetin (**6**), forming prop-1-ene-1,3-diyl diacetate (**7**). Note that compound **7**, which has a mass of 158 uma, exists in two stereoisomers (cis and trans). Moreover, one additional isomer can be envisaged by elimination of a primary ester group (instead of the secondary),

Scheme 2. Gas Chromatogram after Pyrolysis of Neutral Propylene Glycol with Peaks Identified by Mass Spectroscopy[a]

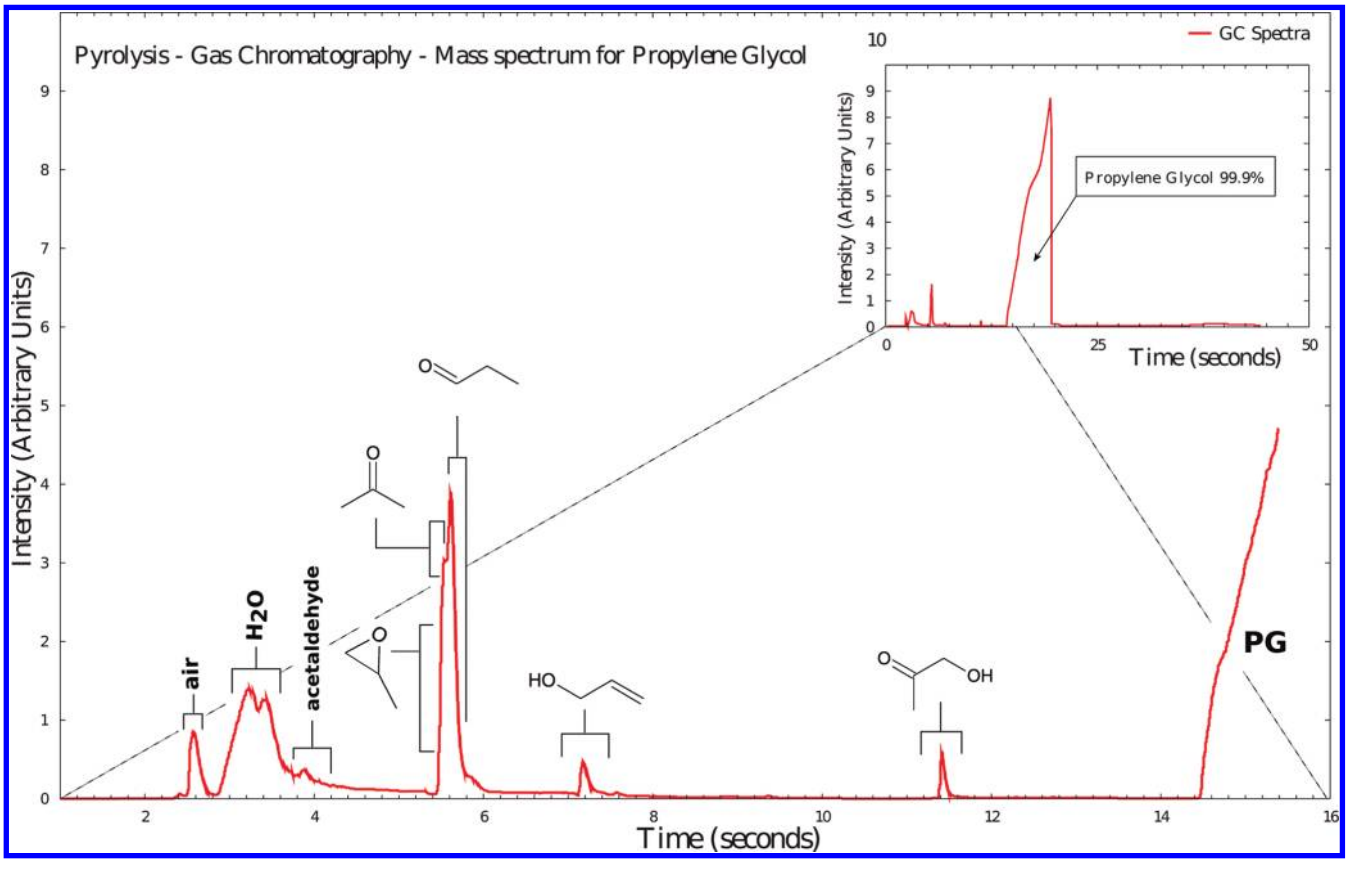

[a]The inset shows the full gas chromatogram of the pyrolytic products, with the percentage of nonpyrolyzed product highlighted.

dx.doi.org/10.1021/jp300997d | J. Phys. Chem. A 2012, 116, 4602−4609

Scheme 3. Branch I: Decomposition of Triacetin (6) via Formation of Prop-1-ene-1,3-diyl Diacetate (7)

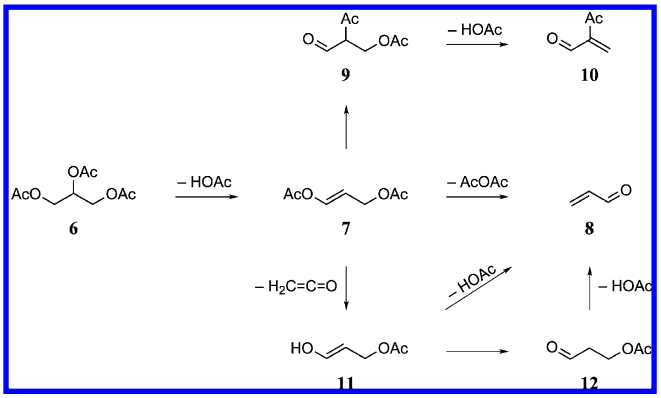

leading to prop-1-ene-2,3-diyl diacetate (not investigated in this work). Intermediate **7** can react further according to three different possible pathways (lowest barrier first, highest barrier last):

- internal rearrangement of **7** into 2-formyl-3-oxobutyl acetate (**9**), with a barrier of 48.3 kcal/mol
- decomposition of **7** into acetic anhydride and acrolein (**8**), with a barrier of 50.2 kcal/mol
- elimination of ethenone from **7** forming 3-hydroxyprop-2-en-1-yl acetate (**11**), with a barrier of 55.4 kcal/mol

Overcoming a barrier of 52.5 kcal/mol, **9** can eliminate acetic acid to form 2-methylidene-3-oxobutanal (**10**). Intermediate **11** represents an enol-type compound. Instead of forming its keto-type equivalent (3-oxopropyl acetate, **12**, barrier height 52.1 kcal/mol), **11** readily decomposes into acrolein (**8**) and acetic acid with a barrier of only 16.5 kcal/mol. If **12** was formed, however, it would also decompose into acrolein and acetic acid (barrier of 55.7 kcal/mol). In Table 2, the thermodynamic and kinetic data are summarized for these steps.

Branch II. Triacetin Decomposition by Elimination of Acetic Anhydride (Scheme 4). In a manner observed similarly for the epoxide formation from both glycerol[7] and propylene glycol, triacetin (**6**) forms glycidyl acetate (**13**) by elimination of acetic anhydride. This epoxide formation step is connected to a barrier of 68.0 kcal/mol, a larger value than the barrier for the competing step **6** → **7** (46.1 kcal/mol). Upon formation, glycidyl acetate (**13**) can decompose according to four possible pathways (lowest barrier first, highest barrier last):

- Internal rearrangement of **13** to 2-methyl-1,3-dioxolane-4-carbaldehyde (**16**, barrier height 56.1 kcal/mol) and subsequent decomposition into acetaldehyde and glycidal (**19**, barrier height 79.5 kcal/mol). Compound **19** can decompose into either methylglyoxal (**24**), malondialde-

Scheme 4. Branch II: Decomposition of Triacetin (6) via Formation of Glycidyl Acetate (13)

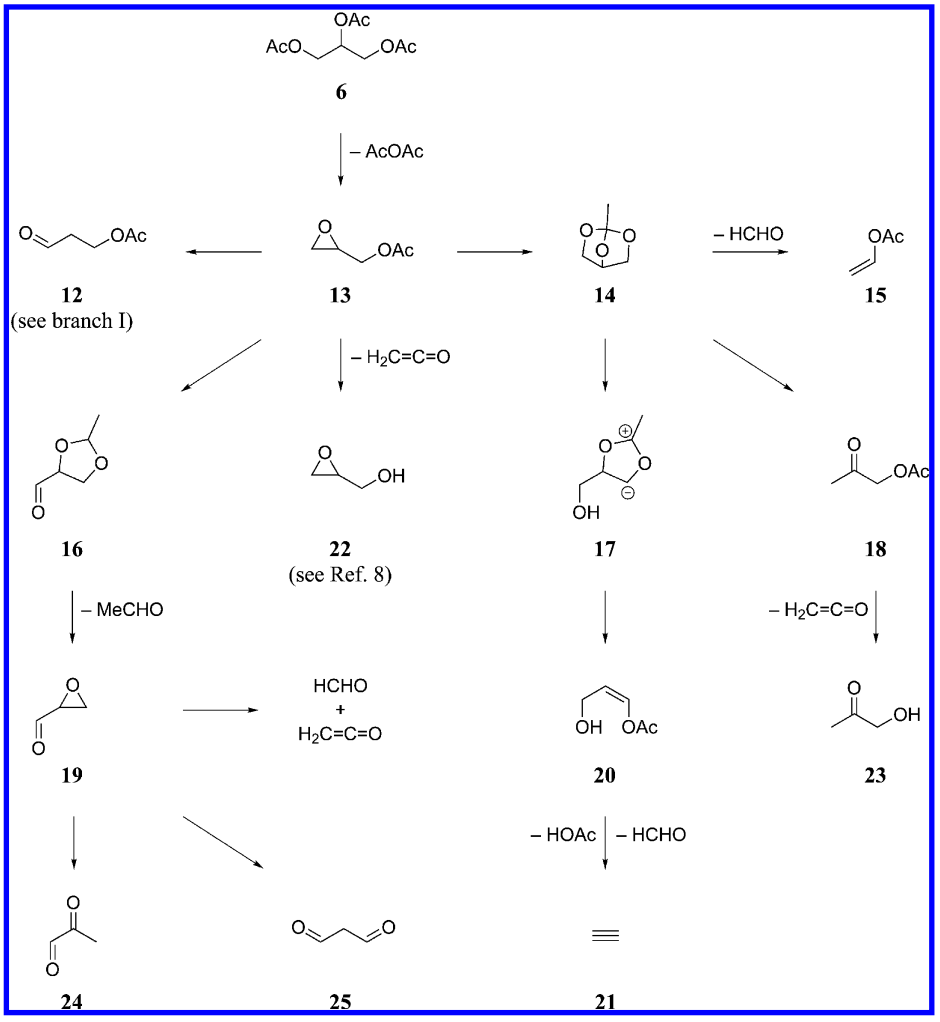

dx.doi.org/10.1021/jp300997d | J. Phys. Chem. A 2012, 116, 4602–4609

Table 2. DFT/PBE0 Total Energy ($\Delta E^{\ddagger}$), Zero-Point Vibrational Energy Corrected ($\Delta E_0^{\ddagger}$), Enthalpy ($\Delta H^{\ddagger}(T)$), and Gibbs Free Energy ($\Delta G^{\ddagger}(T)$) Barrier Heights (kcal/mol) as Well as Rate Constants $k(T)$ (s^{-1}) Computed for the Reaction Steps of the TA Decomposition Branch via Intermediate 7 Depicted in Scheme 3 (T = 800 K)

reaction step	$\Delta E^{\ddagger}$	$\Delta E_0^{\ddagger}$	$\Delta H^{\ddagger}(T)$	$\Delta G^{\ddagger}(T)$	$k(T)$
6 → 7	51.7	47.0	47.1	46.1	4×10^{-0}
7 → 8	49.9	47.8	47.7	50.2	3×10^{-1}
7 → 9	45.7	44.3	43.5	48.3	1×10^{0}
7 → 11	64.4	59.2	59.9	55.4	1×10^{-2}
9 → 10	46.5	46.3	44.2	52.5	7×10^{-2}
11 → 8	18.5	14.8	14.2	16.5	$5 \times 10^{+8}$
11 → 12	56.2	52.0	51.4	52.1	1×10^{-1}
12 → 8	62.1	56.9	57.5	55.7	1×10^{-2}

hyde (**25**) or formaldehyde and ethenone. Overall, the conversion of intermediate **19** into methylglyoxal (**24**, barrier height 59.3 kcal/mol) is the most likely to occur, followed by the decomposition into formaldehyde and ethenone (barrier height 62.9 kcal/mol). Conversion into malondialdehyde (**25**, barrier height 64.4 kcal/mol) is the highest in energy and therefore the least likely to occur.

- internal rearrangement of **13** to 3-oxopropyl acetate (**12**, barrier height 63.7 kcal/mol), which decomposes as described earlier in branch I (Scheme 3)
- internal nucleophilic ring attack of the ester group of **13**, leading to the bicyclic intermediate 1-methyl-2,6,7-trioxabicyclo[2.2.1]heptane (**14**, barrier height 65.8 kcal/mol)
- formation of glycidol (**22**, barrier height 71.0 kcal/mol) via elimination of ethenone from the acetate group

Once formed, intermediate **14** follows one of these reactions (lowest barrier first, highest barrier last):

- ring-opening of **14** to transient species **17** (barrier height 51.4 kcal/mol), which in turn quickly shows another ring-opening to 3-hydroxyprop-1-en-1-yl acetate (**20**, barrier height 3.6 kcal/mol)
- ring-opening of **14**, forming acetonyl acetate (**18**, barrier height 54.4 kcal/mol), which can decompose further into ethenone and 1-hydroxypropan-2-one (**23**, barrier height 67.9 kcal/mol)
- elimination of formaldehyde from **14** and ring-opening to form vinyl acetate (**15**, barrier height 65.5 kcal/mol).

With a barrier of 64.0 kcal/mol, 3-hydroxyprop-1-en-1-yl acetate (**20**) finally decomposes into formaldehyde, acetic acid, and acetylene (**21**). In Table 3 the corresponding thermodynamic and kinetic data are listed for this part of the TA decomposition (Scheme 4).

Branch III. Triacetin Decomposition by Elimination of Ethenone. The elimination of ethenone from acetate groups is a general thermal decomposition pattern known from the literature for acetic acid or acetic anhydride,[26−30] for example. As shown above, we have already seen this type of reaction for the depletion of intermediate **19** and the formation of intermediates **11**, **22**, and **23** with barrier heights between 55 and 71 kcal/mol. Pristine TA is potentially exposed to this decomposition pattern as well. For decomposition into 1,2- or 1,3-diacetin, we computed a Gibbs free energy barrier height of 67 kcal/mol. Although these reactions can compete with the formation of glycidyl acetate (**13**, rate limiting step in the second decomposition branch), they are much slower than the formation of prop-1-ene-1,3-diyl diacetate (**7**, first decomposition branch). We expect virtually no change in the barrier heights for further stepwise decompositions into 1- and 2-monoacetin and, finally, glycerol, which has recently been the subject of another computational study.[7] For these reasons, we consider this part of the triacetin decomposition scheme of minor importance.

Table 3. DFT/PBE0 Total Energy ($\Delta E^{\ddagger}$), Zero-Point Vibrational Energy Corrected ($\Delta E_0^{\ddagger}$), Enthalpy ($\Delta H^{\ddagger}(T)$), and Gibbs Free Energy ($\Delta G^{\ddagger}(T)$) Barrier Heights (kcal/mol) as Well as Rate Constants $k(T)$ (s^{-1}) Computed for the Reaction Steps of the TA Decomposition Branch via Intermediate 13 Depicted in Scheme 4 (T = 800 K)

reaction step	$\Delta E^{\ddagger}$	$\Delta E_0^{\ddagger}$	$\Delta H^{\ddagger}(T)$	$\Delta G^{\ddagger}(T)$	$k(T)$
6 → 13	73.1	70.0	70.0	68.0	5×10^{-6}
13 → 12	69.0	64.9	65.0	63.7	7×10^{-5}
13 → 14	65.6	63.5	62.9	65.8	2×10^{-5}
13 → 16	49.4	48.1	46.0	56.1	8×10^{-3}
13 → 22	72.8	68.9	68.6	71.0	7×10^{-7}
14 → 15	74.9	70.1	71.9	65.5	2×10^{-5}
14 → 17	58.4	53.9	54.3	51.4	2×10^{-1}
14 → 18	65.5	60.1	61.6	54.4	2×10^{-2}
16 → 19	84.3	81.2	81.8	79.5	3×10^{-9}
17 → 20	3.9	3.1	2.2	3.6	$2 \times 10^{+12}$
18 → 23	71.4	66.7	66.8	67.9	5×10^{-6}
19 → 24	64.8	60.7	61.2	59.3	1×10^{-3}
19 → 25	67.9	64.4	64.3	64.4	4×10^{-5}
20 → 21	71.6	65.4	66.3	64.0	5×10^{-5}

Experimental Insights. Similarly to the validation performed for the theoretical investigation of PG, also for TA, upon completion of the computational mapping of all degradation processes we performed pyrolysis−gas chromatography−mass spectrometry studies to validate the simulation framework applied to the decomposition of TA. In Scheme 5, we report the experimental GC spectrum of the pyrolytic products of TA, showing 21 unique peaks: 17 of them assigned on the basis of available reference MS spectrum and 4 reported as unknowns.

The validation of the simulation framework is extremely good: 15 out of 17 assigned experimental peaks have a correspondence with the mapping done by simulations. The experimental data show two compounds, acetone and allyl acetate, which cannot be identified in the degradation steps modeled by our simulations. Nonetheless, the presence of similar compounds like acetonyl acetate (**18**) and prop-1-ene-1,3-diyl diacetate (**7**) leads to the conclusion that acetone and allyl-acetate could be easily formed by bimolecular reactions, maybe involving molecular oxygen, present in the air.

Four major signals remained undetermined from the experimental investigations. In the Supporting Information, we provide the mass spectra for the unidentified peaks **1**, **2**, **3**, and **4**. It is interesting to observe that the unidentified peaks unk**2**, unk**3**, and unk**4** have a unique mass of 158. The parallelism between the existence of those three peaks in the GC spectrum with an assigned mass of 158 and the existence of three possible different isomers of compound **7**, as determined by our simulations frameworks, also with a mass of 158, spontaneously bring us to the hypothesis that unk**2**, unk**3**, and unk**4** can be assigned to the three different isomers of **7**

dx.doi.org/10.1021/jp300997d | J. Phys. Chem. A 2012, 116, 4602−4609

Scheme 5. Gas Chromatogram after Pyrolysis of Neutral Triacetin with Peaks Identified by Mass Spectrometry[a]

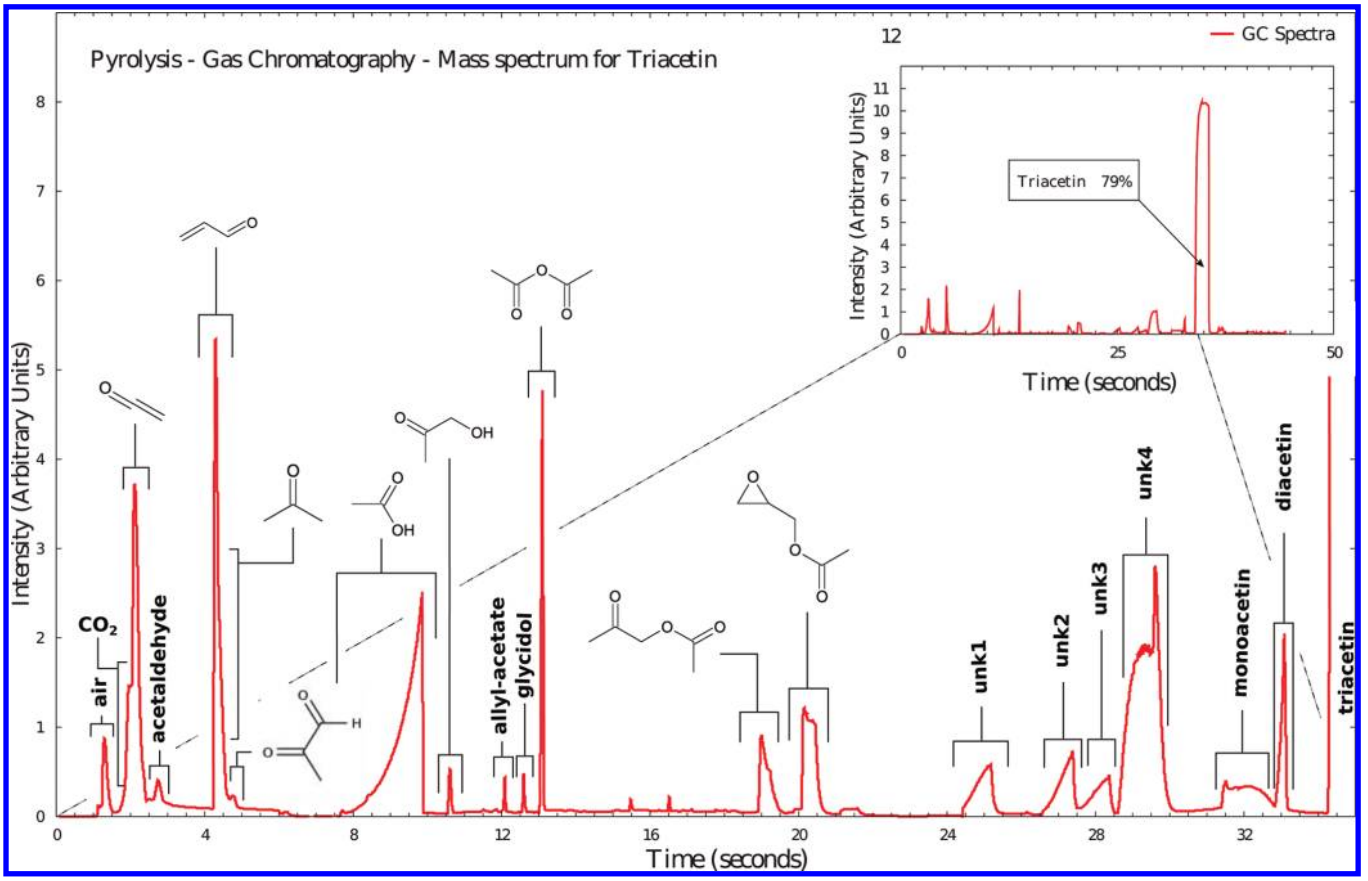

[a]In the inset the full gas chromatogram of the pyrolytic products is shown, with the percentage of nonpyrolyzed product highlighted.

mentioned above. In contrast, unk**1** (see Supporting Information), remains unassigned. Differently from what we determined for propylene glycol, the lower barriers for the primary steps of the TA degradation mechanisms are in good agreement with the lower amount of pure triacetin detected after pyrolysis (79%). Triacetin degrades quickly at high temperature, producing a large series of potentially harmful compounds. The experimental validation for the modeling of TA pyrolysis is extremely good: 15 compounds were matched with the outcomes of the simulations. Moreover, on the basis of the results of our simulation framework, we have offered a very plausible interpretation for three of the four unknown peaks.

CONCLUSIONS

Propylene glycol and triacetin are chemical compounds, commonly used as food additives and potentially exposed to high temperatures during food industry processes, e.g., cooking. Though the usage of the pure chemicals is not considered to be harmful to human beings,[1] little is known about the nature of their thermal degradation products.

In this manuscript, we have applied a novel simulation framework to predict pathways for the thermal decomposition of propylene glycol and triacetin, validating these findings with experimental pyrolysis, gas chromatography, and mass spectrometry. For both TA and PG, the theoretical predictions are in extremely good agreement with the experimental data. Specifically, for TA, which exhibits a more complex decomposition pathway than PG, 15 of the experimental peaks of the GC spectrum immediately matched the results of our modeling investigations. Moreover, our simulation data offered convincing assignments for three out of four unknown experimental peaks.

Consistent with our findings for glycerol,[7] we discovered a new dehydration pathway for neutral propylene glycol based on the formation of propylene oxide. By further decomposition, propanal and minor amounts of acetone are predicted as final degradation products from our modeling. In contrast, triacetin is characterized by elimination of acetic groups, either as acetic acid or acetic anhydride, the first being energetically more accessible. The complete decomposition of TA produces a large series of chemicals, many of them with serious health implications.

From a quantitative point of view, we have computed the kinetic constants for the entire mapping of the decomposition pathways. Triacetin has a higher tendency to decompose than propylene glycol and glycerol because the initial step (**6** → **7**) shows a barrier of 46.1 kcal/mol, less than in the case of glycerol and propylene glycol (66.8 and 66.5 kcal/mol, respectively). Instead, on the basis of the energetics of the rate determining step, propylene glycol exhibits a thermal stability similar to that of glycerol: they tend to decompose slowly even at 800 K. This is in excellent agreement with the experimental data: after 30 s at 800 K, pristine propylene glycol is still present in the mix with an abundance of 99.9%, whereas pristine triacetin is only present with an abundance of 79%.

We therefore can conclude that whenever there is a choice to be made between propylene glycol and triacetin as food additive, and the food is potentially exposed to high

dx.doi.org/10.1021/jp300997d | J. Phys. Chem. A 2012, 116, 4602−4609

temperature processes, e.g., cooking, then propylene glycol may offer advantages as it is intrinsically more stable to pyrolysis. In fact, TA decomposes into a wide range of highly reactive chemical compounds as confirmed by the experimental data.

Moreover, the present study provides a validation of our novel simulation framework employed for predicting thermal decomposition processes.

■ ASSOCIATED CONTENT

Supporting Information

Cartesian coordinates (for transition structures), PBE barrier heights, and mass spectra (for unknown compounds only). This material is available free of charge via the Internet at http://pubs.acs.org/.

■ AUTHOR INFORMATION

Corresponding Author

*E-mail: teo@zurich.ibm.com. Phone: +41 (0) 44 724 8933. Fax: +41 (0) 44 724 8958.

Notes

The authors declare no competing financial interest.

■ ACKNOWLEDGMENTS

We thank David Ghosh and Michel Rotach for their support in performing the experimental validation and Evan Jochnowitz for critically reviewing the manuscript.

■ REFERENCES

(1) US Food and Drug Administration, GRAS database, http://www.fda.gov/Food/FoodIngredientsPackaging/GenerallyRecognizedasSafeGRAS/default.htm.
(2) Mori, K.; Yamada, Y.; Sato, S. *Appl. Catal. A: General* **2009**, *366*, 304−308.
(3) Diaz, E.; Sad, M. E.; Iglesia, E. *ChemSusChem* **2010**, *3*, 1063−1070.
(4) Dai, Z.; Hatano, B.; Tagaya, H. *Appl. Catal. A: General* **2004**, *258*, 189−193.
(5) Long, H.; Yulei, Z.; Hongyan, Z.; Guoqiang, D.; Yongwang, L. *Catal. Lett.* **2009**, *131*, 312−320.
(6) Rungnim, C.; Ruangpornvisuti, V. *J. Comput. Chem.* **2005**, *26*, 1592−1599.
(7) Laino, T.; Tuma, C.; Curioni, A.; Jochnowitz, E.; Stolz, S. *J. Phys. Chem. A* **2011**, *115*, 3592−3595.
(8) Sun, W.; Liu, J.; Chu, X.; Zhang, C.; Liu, C. *J. Mol. Struct.: THEOCHEM* **2010**, *942*, 38−42.
(9) Laio, A.; Parrinello, M. *Proc. Natl. Acad. Sci. U. S. A.* **2002**, *99*, 12562−12566.
(10) Iannuzzi, M.; Laio, A.; Parrinello, M. *Phys. Rev. Lett.* **2003**, *90*, 238302−238306.
(11) Henkelman, G.; Uberuaga, B. P.; Jónsson, H. *J. Chem. Phys.* **2000**, *113*, 9901.
(12) Adamo, C.; Barone, V. *J. Chem. Phys.* **1999**, *110*, 6158.
(13) Eyring, H. *J. Chem. Phys.* **1935**, *3*, 492.
(14) Evans, M. G.; Polanyi, M. *Trans. Faraday Soc.* **1935**, *31*, 875.
(15) Evans, M. G.; Polanyi, M. *Trans. Faraday Soc.* **1937**, *33*, 448.
(16) Laidler, K. J.; King, M. C. *J. Phys. Chem.* **1983**, *87*, 2657.
(17) Truhlar, D. G.; Hase, W. L.; Hynes, J. T. *J. Phys. Chem.* **1983**, *87*, 2664.
(18) Perdew, J. P.; Burke, K.; Ernzerhof, M. *Phys. Rev. Lett.* **1996**, *77*, 3865−3868.
(19) Troullier, N.; Martins, J. L. *Phys. Rev. B* **1991**, *43*, 1993.
(20) CPMD, Copyright Max Planck Institut für Festkörperforschung Stuttgart 1997−2001, Copyright IBM Corp. 1990−2010. http://www.cpmd.org.
(21) The CP2K developers group, code released under GPL license, freely available at http://www.cp2k.org.
(22) Stewart, J. J. P. *J. Mol. Model.* **2007**, *13*, 1173.
(23) Martyna, G. J.; Tuckerman, M. E. *J. Chem. Phys.* **1999**, *110*, 2810.
(24) Gonzalez, C.; Schlegel, H. B. *J. Chem. Phys.* **1989**, *90*, 2154.
(25) *Wiley Registry of Mass Spectral Data 9th Ed. with NIST 2008*; John Wiley and Sons: New York, 2011.
(26) Nguyen, M. T.; Sengupta, D.; Raspoet, G.; Vanquickenborne, L. G. *J. Phys. Chem.* **1995**, *99*, 11883−11888.
(27) Moreira, I. P. R *J. Mol. Struct.: THEOCHEM* **1999**, *466*, 119−126.
(28) Takahashi, O.; Itoh, K.; Saito, K. *J. Mol. Struct.: THEOCHEM* **2002**, *584*, 249−256.
(29) Metcalfe, W. K.; Simmie, J. M.; Curran, H. J. *J. Phys. Chem. A* **2010**, *114*, 5478−5484.
(30) Akao, M.; Saito, K.; Okada, K.; Takahashi, O.; Tabayashi, K. *Ber. Bunsen-Ges. Phys. Chem.* **1996**, *100*, 1237−1241.